Effects of the Spatial Nonuniformity of Optical Transverse Modes on the Modulation Response of Vertical-Cavity Surface-Emitting Lasers

Yang Liu, Wei-Choon Ng, *Member, IEEE*, Benjamin Klein, and Karl Hess, *Fellow, IEEE*

***Abstract*—We present detailed numerical simulations to clarify the important role that the nonuniformity of the transverse optical mode plays for the high-speed response of oxide-confined vertical-cavity surface-emitting lasers (VCSELs). The comprehensive laser diode simulator, Minilase, as well as a one-dimensional rate equation model are used as simulation tools. It is demonstrated that, due to the nonuniform optical intensity, carriers at different locations in the quantum well have different stimulated recombination rates, and therefore exhibit different dynamic responses to small signal modulation. This nonuniformity causes an overdamping of the relaxation oscillation, as well as a low-frequency roll-off of the modulation response. Due to this nonlinear effect, the intrinsic maximum bandwidth of VCSELs with oxide confined apertures is shown to be much smaller than predicted by the conventional rate equation model which assumes uniform optical intensity. We further demonstrate that this damping effect can be greatly reduced by restricting the current injection to be well within the transverse optical field. This is achievable by using tapered oxides to make the electrical aperture smaller than the optical aperture, and thereby improves the modulation bandwidth significantly.**

***Index Terms*—Amplitude modulation, dynamic response, nonlinear gain suppression, spatial hole-burning, surface-emitting lasers.**

I. Introduction

VERTICAL-CAVITY surface-emitting lasers (VCSELs) have attracted great interest for applications in high-speed optoelectronics because of the possible single-mode operation and good scalability and integrability with other optoelectronic components. Recent developments in fabrication technology have enabled great progress in the modulation bandwidth and modulation efficiency of VCSELs [1], [2]. In practice, the ringing associated with the underdamping of the relaxation oscillation can yield undesirable eye diagrams, and a compromise may be needed between lower relaxation frequency and increased damping factor for improved eye patterns. However, the overdamping caused by various nonlinear effects limits the intrinsic maximum bandwidth of VCSELs, and better understanding of such effects hence becomes an absolute necessity in order to achieve further improvements for applications operating at tens of gigahertz. In the literature, various gain suppression effects in laser diodes have been extensively examined, including carrier transport, spectral hole-burning, carrier heating, lattice heating, and spatial hole-burning (SHB) [3]–[10]. The SHB effect is closely related to the nonuniformity of the transverse-mode intensity. In [7] and [8], it has been reported that SHB plays an important role in the multitransverse-mode competition due to sharing of the carrier reservoir of large aperture VCSELs. Yu *et al.* have developed a rate equation model to simulate various effects including SHB on VCSELs' modulation responses [9], [10]. However, the nonlinear effects that are directly caused by the nonuniform mode intensity are not clarified in their work. In our study, detailed numerical simulations and theoretical analysis are carried out for strongly index-guided, single-mode VCSELs. For this type of device, the nonuniform transverse mode is a very important source of the overdamping in the modulation response, and this effect has not been treated in detail in VCSEL modeling and simulation so far. Its influence on the modulation response can be explained by the fact that the stimulated recombination rate of quantum well (QW) carriers is proportional to the local mode intensity. Therefore, when the device is directly modulated, QW carriers in different regions will exhibit quite different dynamic responses due to the variation in the mode intensity. As a result, the overall relaxation oscillation will be overdamped. This effect has been experimentally confirmed for a two-section distributed feedback (DFB) laser [11]. By adjusting the photon density distribution in the two sections, it was demonstrated that the relaxation frequency and damping factor can be changed even if the output power is kept constant. The overdamping effect was not very significant in their work since both the spatial gradient of the optical mode and the photon density were relatively small [11]. However, for small aperture VCSELs, the HE11-like transverse optical mode is tightly confined to a very small region due to strong index guiding, and this strong nonuniformity has a significant influence on the dynamic behavior of VCSELs. Some preliminary results on this effect have been reported in our previous work [12], [13]. Minilase has been used extensively [12] to simulate the effects of electronic transport on the modulation response of VCSELs, including the effects of diffusion capacitance, of the lateral diffusion of QW carriers and of the nonuniform optical field. This work focuses on the dynamic effects resulting from

Manuscript received April 24, 2002; revised September 9, 2002. This work was supported by the Office of Naval Research under Contract N0014-98-1-0604.

Y. Liu is with the Department of Physics, Beckman Institute, University of Illinois at Urbana–Champaign, Urbana, IL 61801 USA (e-mail: yangliu1@uiuc.edu).

W.-C. Ng and K. Hess are with the Department of Electrical and Computer Engineering, Beckman Institute, University of Illinois at Urbana–Champaign, Urbana, IL 61801 USA.

B. Klein was with the Department of Electrical and Computer Engineering, Beckman Institute, University of Illinois at Urbana-Champaign, Urbana, IL 61801 USA. He is now with NIST, Boulder, CO 80305 USA.

Digital Object Identifier 10.1109/JQE.2002.806205

the nonuniform optical mode. Further simulation results, as well as an in-depth theoretical analysis, are presented here.

The major tool used in our simulations is Minilase, which is a comprehensive laser diode simulator based on fundamental principles of laser physics and includes various nonlinear gain effects [6]. Recently, it has been extended to simulate VCSEL structures [14] and good agreement with experiments has also been achieved for the modulation response [12]. A simple rate equation model along the radial direction has also been developed to better explain the role of nonuniform modes in the dynamic response. Unlike the conventional rate equation model, which assumes uniform mode intensity within the QW plane, our one-dimensional (1-D) model takes into account the variation of mode intensity in the stimulated recombination. Strong overdamping is still observed in the modulation response, although no gain suppression factor is explicitly introduced in this model, which is attributed to our inclusion of the nonuniform mode intensity.

The paper is organized as follows. In Section II, basic principles implemented in Minilase are briefly reviewed. Following that, a short description of our rate equation model is given. Simulation results for oxide-confined VCSELs are presented in Section III. A significant overdamping in the relaxation oscillation due to the nonuniformity of the transverse mode is demonstrated, and a significant reduction in the modulation bandwidth is reported for VCSELs with small oxide apertures. Due to the limit of this overdamping effect, the intrinsic maximum bandwidth of VCSELs with oxide confined apertures is shown to be much smaller than predicted by the conventional rate equation model. Furthermore, it is demonstrated that the nonlinear effect due to nonuniform modes can be greatly reduced by making the electrical aperture smaller than the optical aperture. A possible design technique to achieve this improvement is to use a tapered oxide aperture, as shown by Minilase simulations. In addition to the numerical simulations, a closed-form expression of the modulation response is derived in the Appendix for a simplified 1-D rate equation model, which further clarifies that the spatial nonuniformity of the mode leads to significant nonlinear effects.

II. Models

The conventional rate equation model has been described in many textbooks [15], [16]. The photon density S is assumed to be uniform within the QW plane. Various nonlinear gain effects are included phenomenologically by using the gain expression $g(S) = g_0/(1+\epsilon S)$ where g_0 is the material gain, and ϵ is the phenomenological gain suppression factor. The modulation response as a function of the modulation frequency f usually has the form

$$\frac{s(f)}{j(f)} \propto \left[(f^2 - f_r^2) + if\gamma/(2\pi)\right]^{-1} \tag{1}$$

as obtained by small-signal analysis. Here, $s(f)$ and $j(f)$ are the small-signal terms of photon density and current density respectively, f_r is the relaxation frequency, and γ is the damping factor. As the output power increases, γ rises proportionally to f_r^2, and the so-called K factor is usually introduced as the constant of proportionality. The conventional rate equation shows that $K = 4\pi^2[\tau_p + \epsilon/(v_g g')]$, where τ_p is the photon lifetime, v_g is the group velocity of light, and g' is the differential material gain. The relaxation oscillation is completely damped due to the increasing damping factor at very high output power, and the bandwidth saturates at a maximum value which is determined by $f_{\max} = 2\pi\sqrt{2}/K$ [15].

Minilase uses a very different approach [6]. Poisson and continuity equations for both electrons and holes are self-consistently solved using Newton method. Drift–diffusion transport is assumed for bulk carriers as well as the lateral transport of QW carriers. At the heterojunction interfaces, the carriers thermionically transport from one material to the other. Inside the QW, carriers are separated into two types: those occupying continuum and those occupying bound states, each with distinct quasi-Fermi levels. Scattering between these states through carrier–carrier and carrier–phonon interactions is also included to connect the population of the continuum and bound states. To simulate the carrier transport in energy space, a 1-D Boltzmann equation is solved for QW carriers. In addition, an eight-band $k \cdot p$ method has been incorporated to calculate QW band structure and optical matrix elements. The band-gap renormalization due to many-body effects is included in the local density approximation [17]. The carrier density and electrostatic potential obtained from the Newton solver are used as the input for the $k \cdot p$ solver. In return, the updated band-gap energy and envelope functions are fed back to the Newton solver. Minilase iterates between these two solvers until convergence to ensure self-consistency. Two optical solvers, one based on the Green's function method [18] and one based on the self-consistent effective index method [19], have been developed and incorporated into Minilase to compute the central frequency, optical confinement factor, transverse-mode intensity, and photon lifetime. The modulation response is obtained through time-dependent simulation after applying a small step on top of the steady-state current bias [6]. Thus, as a quasi-three-dimensional simulator, Minilase has carefully accounted for the physics that result in nonlinear gain effects, such as nonuniform modes, carrier transport, carrier heating, and spectral hole-burning. We have turned off the energy space solver in order to focus on the effects due to nonuniform mode intensity. A Fermi distribution is therefore assumed to describe the QW carriers in the simulations that are reported here. As a result, spectral hole-burning and carrier-heating effects are not included. However, other gain suppression effects due to carrier transport are fully included and are shown to have significant influence on the modulation response of VCSELs [12]. The simulations were performed on a DEC Alpha 500-MHz workstation, and it takes $\sim$1 h for a time-dependent run.

To extract and crystallize the physics of the simulation results that are obtained from Minilase and to clarify the role of mode nonuniformity in the high-speed performance of VCSELs, we have also developed a 1-D rate equation model, which consists of the photon rate equation and the carrier continuity equation, describing the spatially varying carrier and optical mode distributions within the QW. Only one type of carrier is considered and, therefore, charge neutrality is assumed. Generally speaking, the laser field has a spatiotemporal amplitude. To make device-level simulations feasible, the photon rate equation

has been used based on a widely accepted simplification, i.e., the space-time field can be Fourier decomposed into a small set of well chosen modes with slowly varying time-dependent amplitudes. This is justifiable because the modulation frequencies are far below the optical frequencies. Since we are only considering single-mode and strongly index-guided structures, only the fundamental mode has been included. This model is sufficient to capture the basic physics related to mode nonuniformity. For a device with radius R_D and QW thickness d, the rate equations are written as

$$\frac{\partial n(r,\,t)}{\partial t} = \frac{j(r,\,t)}{qd} - \frac{n(r,\,t)}{\tau_r} + D\left[\frac{1}{r}\frac{\partial n(r,\,t)}{\partial r} + \frac{\partial^2 n(r,\,t)}{\partial r^2}\right] - \alpha\eta v_g g'[n(r,\,t) - n_{tr}]S(t) \tag{2}$$

and

$$\frac{\partial S(t)}{\partial t} = \frac{\Gamma_z}{R_D^2}\int_0^{R_D} \alpha v_g g'[n(r,\,t) - n_{tr}]S(t)\cdot dr^2 - \frac{S(t)}{\tau_p} + \beta R_{sp} \tag{3}$$

where r is the radial distance from the axis of symmetry, $n(r,\,t)$ is the QW carrier density as a function of position and time, and $S(t)$ is the average photon density, i.e., $S(t) = N_{ph}/V$, where N_{ph} is the photon number and V is the volume of the entire cavity. The first term in Eqn. (2) corresponds to the current injection into the QW, and the current density $j(r,\,t)$ is modeled as [20]

$$j(r,\,t) = \begin{cases} j_0(t), & r < R_a \\ j_0(t)\exp[-(r - R_a)/l_D], & r \geq R_a \end{cases} \tag{4}$$

where R_a is the oxide aperture radius and l_D is the lateral diffusion length for carriers traveling across the separate confinement heterojunction (SCH) region. This model of current injection is reasonable, as has been confirmed by simulation results from Minilase. τ_r in the second term of (2) is the carrier lifetime due to spontaneous emission and dark recombination. The carrier lateral diffusion is treated in the third term, and the diffusion constant D is calculated from the Einstein relation as $\mu k_B T/q$, where μ is the mobility, k_B is the Boltzmann constant, T is the temperature, and q is the elementary charge.[1] The major improvement over the conventional rate equation model comes in the treatment of stimulated recombination in the last term of (2) and the first term of (3). In calculating these terms, the ratio of the local mode intensity to the average mode intensity $|E(z,\,r)|^2/\langle|E(z,\,r)|^2\rangle$ needs to be used as a prefactor to account for the dependence of the stimulated recombination rate on the local field intensity. By assuming separability of the optical field $E(z,\,r) \approx E_z(z)\cdot E_r(r)$, α and η are introduced as the radial and longitudinal components of $|E(z,\,r)|^2/\langle|E(z,\,r)|^2\rangle$, respectively

$$\frac{|E(z,\,r)|^2}{\langle|E(z,\,r)|^2\rangle} \approx \frac{|E_z(z)|^2}{\langle|E_z(z)|^2\rangle_z}\cdot\frac{|E_r(r)|^2}{\langle|E_r(r)|^2\rangle_r} = \frac{|E_z(z)|^2}{\langle|E_z(z)|^2\rangle_z}\cdot\frac{R_D^2|E_r(r)|^2}{\int_0^{R_D}|E_r(r)|^2\,dr^2} \equiv \eta\cdot\alpha. \tag{5}$$

[1]Minilase uses a more precise relation obtained from the Fermi distribution.

The longitudinal ratio $\eta \equiv |E_z(z)|^2/\langle|E_z(z)|^2\rangle_z$ depends on position and thickness of the QW, and the overall effect is that the modal gain is enhanced by a factor of η [21]. For VCSEL structures studied in this work, η is taken to be 2 because the QW is very thin and placed at the peak position of the standing wave pattern in the longitudinal direction. It should be noted that η does not explicitly appear in the first term of the photon rate equation [(3)] because it has already been included in the vertical optical confinement factor Γ_z as

$$\Gamma_z \equiv \frac{\int_{QW} dz|E_z(z)|^2}{\int_{\text{cavity}} dz|E_z(z)|^2} \approx \frac{d\cdot|E_z|^2_{\text{QW}}}{L\cdot\langle|E_z(z)|^2\rangle_z} = \frac{d}{L}\cdot\frac{|E_z|^2_{\text{QW}}}{\langle|E_z(z)|^2\rangle_z} = \frac{d}{L}\cdot\eta \tag{6}$$

where d and L are the thickness of the QW and the entire cavity respectively, and $|E_z(z)|^2$ is assumed to be constant across the thin QW layer. In the transverse direction, $\alpha \equiv [R_D^2|E_r(r)|^2]/[\int_0^{R_D}|E_r(r)|^2\,dr^2]$ is the local optical field normalized in the QW plane and approximated by a Gaussian, i.e., $\alpha \propto \exp[-(r/R_w)^2]$, where R_w is the beam waist. α is normalized by the condition $\int_0^{R_D}\alpha\cdot dr^2/R_D^2 = 1$, as can be seen from its definition. Simulations with the mode solvers of Minilase show that a Gaussian mode is a good approximation to the exact fundamental mode of the particular oxide-confined VCSEL structure studied here. The "cold" cavity mode is used throughout and gain-guiding effects are neglected. This is a fairly reasonable simplification because index guiding is a far more dominant mechanism for small-aperture oxide confined structures that are studied in this paper. In the photon rate equation, τ_p is the photon lifetime to account for the total cavity losses, including mirror loss, internal loss, scattering loss and diffraction loss. βR_{sp} is the spontaneous emission coupled into the lasing mode, which is ignored in our rate equation simulations since we are only considering biases well above lasing threshold. This set of rate equations is discretized over the radial direction r, as well as in time domain t, using a finite difference time-marching method. At the device boundaries, we assume $\partial n/\partial r = 0$, ($r = 0$ or R_D). The modulation response is also obtained from time-dependent simulation, which is similar to the treatment in Minilase. It is worth noting that this 1-D model assumes a linear relationship between the material gain and the carrier density $g = g'(n - n_{tr})$, where n_{tr} is the carrier density at transparency, and no gain suppression factor ϵ is explicitly included. Hence, the nonlinear gain effects included in this model can only be associated with the nonuniform mode.

III. Simulation Results and Discussion

All Minilase simulations presented in this paper are based on a double oxide-confined, 1-λ cavity VCSEL structure, which has experimentally exhibited a bandwidth greater than 16 GHz [1]. The Minilase electrical solver simulates only the active cavity between the top and the bottom oxide layers, since we are mainly interested in the intrinsic dynamic response. However, the Minilase optical solvers take into account the entire device including the upper and lower DBR stacks. The active layer consists of a single 80-Å $In_{0.2}Ga_{0.8}As$ QW operating

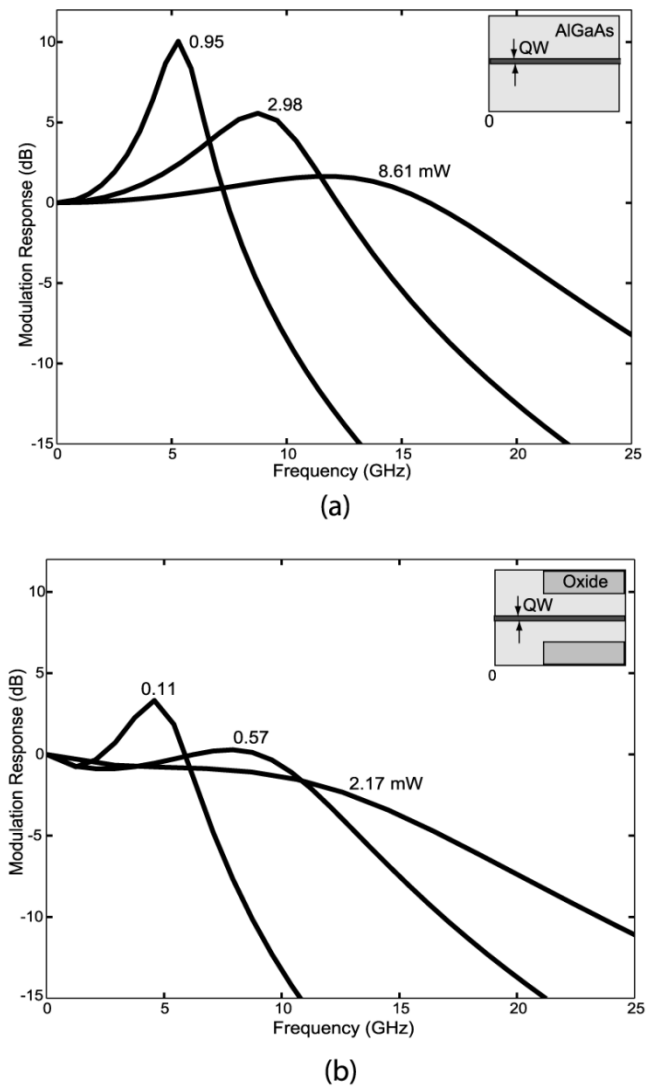

Fig. 1. Modulation responses simulated by Minilase for: (a) an artificial VCSEL assuming uniform current injection and optical transverse mode and (b) a realistic double-oxide-confined VCSEL with an aperture radius of 1.8 μm. The response curves are labeled by their output power.

at 980 nm. The separate confinement region consists of a 140-nm layer of intrinsic and ungraded $Al_{0.1}Ga_{0.9}As$ on each side. The oxide aperture layer is composed of $Al_{0.98}Ga_{0.02}As$ with a doping density of 1×10^{18} cm^{-3} on both the p- and n-side. A square aperture of 3×3 μm^2 has been used in the experiment [1]. However, cylindrical symmetry is assumed in the simulations to reduce the computation volume, and a default aperture radius of 1.8 μm is used to give approximately the same aperture area. The oxide aperture radius is also varied in our simulations for the purpose of comparison.

Minilase has been used to simulate the modulation response for two different structures to demonstrate the effects due to optical mode nonuniformity, and the results are shown in Fig. 1. Device (a) is an artificial device with no oxide confinement and the radius of the device is 4 μm, as shown in the inset of Fig. 1(a). Both the current injection and the transverse optical mode are assumed to be constant along the transverse direction. Simulations for this device are essentially 1-D along the vertical direction and therefore SHB does not occur in this case. It is seen that the response curves of Fig. 1(a) exhibit very strong relaxation oscillations and a bandwidth greater than 20 GHz is approached as the output power increases. Device (b) is a realistic double oxide-confined device with oxide aperture radius equal to 1.8 μm, as shown in the inset of Fig. 1(b). The nonuniformity of the mode intensity is very significant in this small-apertured structure. The simulated responses are plotted in Fig. 1(b) and a severe overdamping in the relaxation oscillation is observed for this set of curves. A low-frequency roll-off is also visible. This overdamping effect cannot be attributed to the lateral transport of QW carriers. Previous work based on a rate equation model has demonstrated that the lateral diffusion within the QW does not have a significant influence on VCSEL's relaxation frequency when the diffusion constant is varied within a reasonable range [10]. Minilase simulations have confirmed this observation and shown that the lateral diffusion of QW carriers only slightly dampens the relaxation peak, but does not significantly affect the modulation bandwidth for realistic mobility values [12]. Thus, the huge overdamping effect observed for device (b) can only be explained by the different dynamic behavior of the QW carriers. From (2), we see that the stimulated recombination rate of the QW carriers is a function of position and can be expressed as $\tau_{st}^{-1} = \alpha\eta v_g g' S$. If we artificially divide the VCSEL into many slices laterally, and view each slice as an individual "laser," the relaxation frequency for each small "laser" segment can be expressed as

$$f_r^c(r) = (2\pi)^{-1}\sqrt{\frac{1}{\tau_{st}}\cdot\frac{1}{\tau_p}} = (2\pi)^{-1}\sqrt{\frac{\alpha\eta v_g g' S}{\tau_p}}. \quad (7)$$

Since the optical field intensity α is quite nonuniform, $f_r^c(r)$ varies with position. Consequently, carriers at different locations will have very different dynamic responses, and the total modulation response will be overdamped.

We have also simulated the variation of the electron density as a function of time after adding a small current step to the steady-state bias in device (b), as plotted in Fig. 2. The difference in the

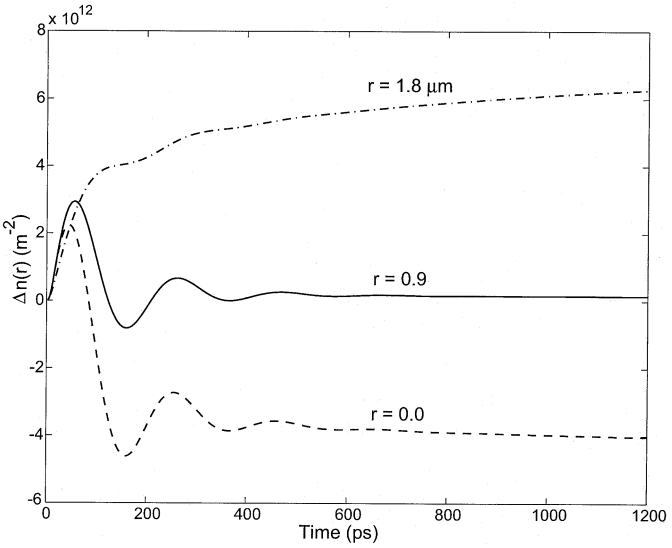

Fig. 2. Variation of the electron density as a function of time at different locations of the QW, after a small current step is applied to the steady-state current bias. The simulation is performed with Minilase for a realistic double oxide-confined VCSEL with an aperture radius of 1.8 μm.

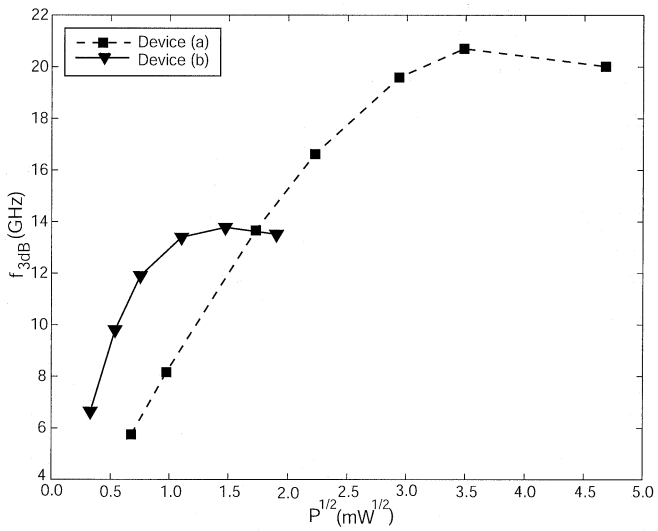

Fig. 3. Simulated 3-dB bandwidth as a function of square root of the output power. The simulation is performed with Minilase for devices identical to those of Fig. 1.

dynamic behavior of carriers at different radial locations is evident in this figure. When the current bias is increased, a larger spatial hole is burned in the central region because the total gain is pinned to the cavity loss above threshold. This explains why the carrier concentration at the central region relaxes to a lower steady-state value, while the opposite is true for the carrier density at the outer region. It is clearly shown that, although the carriers at the central region display strong oscillation behavior, the strength of the relaxation oscillation is very weak at the position $r = 1.8$ μm, which is the edge of the oxide aperture. This indicates that the carriers at the outer region respond to the modulation much slower than those close to the central region.

Fig. 3 shows the simulated 3-dB bandwidth $f_{3\,\mathrm{dB}}$ as a function of the square root of the output power P for the same two devices depicted in Fig. 1. The bandwidth of device (b) is higher than that of device (a) at low output power. This can be explained by the fact that the output power is proportional to the square root of the average photon density, while the relaxation frequency depends on the distribution of the local photon density. For device (b), the optical mode is tightly confined to the central region. As a first-order approximation, it can be viewed as a mode with uniform intensity in the small central region and zero intensity in the outer region of the device. Thus, if the two devices have the same averaged photon density, the actual local density at the central region in device (b) is much higher than that of device (a). Therefore, the relaxation frequency of device (b) is higher than that of device (a) at low output power. Nevertheless, as the output power increases, effects due to the nonuniformity of the mode start to play an important role. Due to this nonlinear effect, the modulation response in device (b) dampens very quickly, and the bandwidth saturates at about 14 GHz. In contrast, device (a) has a small bandwidth at low output power, but the damping of its response is small, and hence $f_{\max} > 20$ GHz can be attained.

As mentioned in Section II, the effects due to carrier transport in the vertical direction are accounted for by Minilase. To better explain and separate the above results from Minilase

TABLE I
VALUES OF PARAMETERS USED IN SIMULATIONS WITH THE 1-D RATE EQUATION MODEL

q	$1.6 \times 10^{-19}\ C$	μ	$0.05\ m^2/V \cdot s$
d	80 Å	R_D	$6\ \mu m$
k_BT	$1.38 \times 10^{-23} \cdot 300\ J$	v	$3 \times 10^8/3.6\ m/s$
τ_r	$1\ ns$	n_{tr}	$1 \times 10^{18}\ cm^{-3}$
Γ_z	0.02	τ_p	$6\ ps$
g'	$1 \times 10^{-19}\ m^2$	l_D	$1\ \mu m$
η	2		

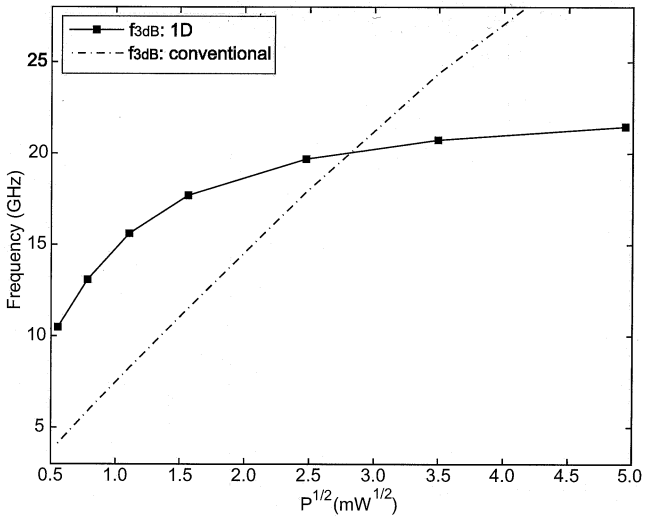

Fig. 4. 3-dB bandwidth as a function of the square root of output power from the 1-D rate equation simulation (solid line) and the conventional rate equation (dashed line), respectively.

simulations, further studies have been performed using the 1-D rate equation model introduced in Section II. The modulation response at various values of output power is obtained from time-dependent simulations for a device with an oxide aperture radius $R_a = 1.8$ μm. The beam waist of the Gaussian mode R_w is set to 1.1 μm by fitting to the exact HE11-like mode calculated by mode solvers. All the values of the other parameters used in the simulations are tabulated in Table I. The simulated 3-dB bandwidth obtained from the 1-D model as a function of the square root of the output power is plotted in Fig. 4. For comparison purposes, simulation results from the conventional rate equation are also obtained by using a uniform transverse-mode profile in the 1-D rate equation model,[2] and the bandwidth $f_{3\,\mathrm{dB}}$ is shown in this figure. Comparing these results with those obtained from Minilase in Fig. 3, one sees that the rate equation model gives a higher bandwidth, which is reasonable since the gain suppression effect due to vertical carrier transport is absent in this model. Nevertheless, a similar trend is observed for $f_{3\,\mathrm{dB}}$,

[2]The modal gain enhancement due to the longitudinal factor η is, therefore, also included for these simulations.

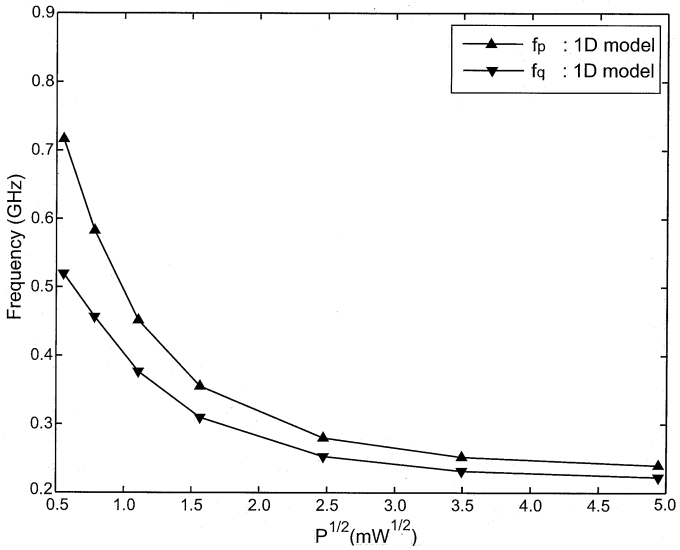

Fig. 5. The additional zero (f_p) and pole (f_q) in the modulation response [(8)] from 1-D rate equation simulations at various values of output power.

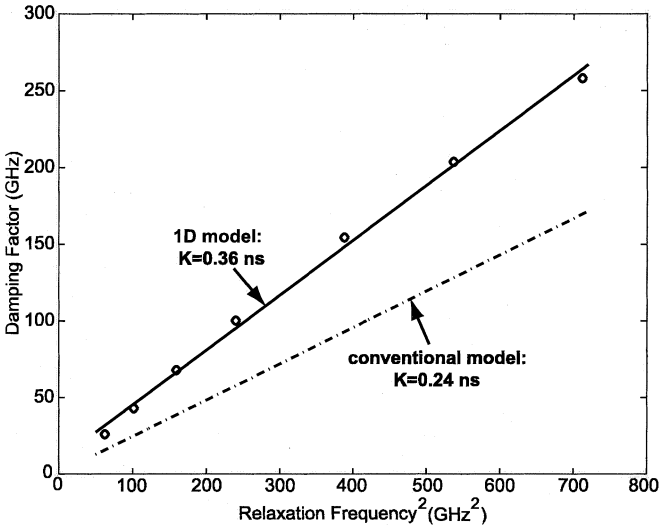

Fig. 6. Damping factor as a function of the square of the relaxation frequency. The "circles" correspond to 1-D rate equation model result, where f_r^* and γ^* are obtained by fittings using (8). Solid line corresponds to a linear fit of γ^* and f_r^{*2}. Dashed line corresponds to the results from the conventional model.

as shown in Fig. 4. The 1-D model gives a relatively high bandwidth for low output power, but its increase with output power saturates very quickly; therefore, the nonuniform mode intensity limits the intrinsic maximum bandwidth to a much lower value as compared to that predicted by the conventional rate equation model. For this 1.8-μm aperture device, it can be seen that the intrinsic maximum bandwidth is reduced to be less than 25 GHz.

To obtain further insight into the underlying dynamics, a closed-form expression of the modulation response has been derived for this 1-D model after two further simplifications: neglecting the diffusion term and assuming uniform current injection, as shown in the Appendix. As can be seen from (A.8), the modulation response at very low output power has the form of (1) as in the conventional rate equation model, except that the transverse optical mode intensity is assumed to be uniform in the central region defined by $r < \sqrt{2}\,R_w$ and zero outside. The modal gain enhancement due to the longitudinal factor η has also been accounted for here. This result supports our previous explanation of Fig. 3. As the output power increases, it can be seen from (A.10) that an additional pole (f_q) and an additional zero (f_p) are introduced, and the proportionality between γ^* and f_r^*, i.e., the K actor, will change due to the nonlinear effects of the nonuniform mode. To obtain f_p, f_q, f_r^*, and γ^*, the simulated response curves from the original 1-D model is fitted by using the expression

$$\left|\frac{s(f)}{j(f)}\right| \propto \left[\frac{f^2+f_p^2}{f^2+f_q^2}\cdot\frac{1}{\left(f^2-f_r^{*2}\right)^2+f^2\gamma^{*2}/(2\pi)^2}\right]^{1/2} \tag{8}$$

which is directly derived from (A.10). Using this expression instead of (1) produces qualitative improvements for fitting the simulated modulation responses. The fitted f_p and f_q at various pumping levels are plotted in Fig. 5. Both are within the low-frequency range ($\lesssim$1 GHz in this figure) and f_q is generally smaller than f_p. As is well known from the linear response theory, the pole f_q causes a $-$20-dB/decade decay in the response for $f > f_q$, while the zero f_p leads to a 20-dB/decade rise for $f > f_p$. Since we have $f_q < f_p$, the overall effect is a low-frequency roll-off, as observed in Fig. 1(b).[3] It is also evident that both f_p and f_q decrease as output power increases, which agrees with the trend of Fig. 1(b).

The damping factor is plotted as a function of the square of the relaxation frequency for the two rate equation models in Fig. 6. According to the conventional model, the K factor and the maximum bandwidth are calculated to be 0.24 ns and 37.5 GHz, respectively, for $\tau_p = 6$ ps and $\epsilon = 0$ cm^3. A fairly good linear relation between γ^* and f_r^{*2} is also observed for the 1-D model results, and a linear fit is therefore performed to give a much larger K factor of 0.36 ns. Therefore, the contribution to the K factor due to the nonuniform optical intensity is $K^* = 0.12$ ns, and the corresponding effective nonlinear gain parameter is $\epsilon^* = K^* \times (\eta v_g g')/(4\pi^2) \approx 5\times 10^{-17}$ cm^3. However, it should be noted that ϵ^* is a phenomenological factor for the purpose of comparison only. It depends on the device structure and is not a material parameter. This value is significant compared to the nonlinear gain factor of about 0.9×10^{-17} cm^3 as obtained for hot-carrier and spectral hole burning in conventional lasers [22].[4] Consequently, the corresponding maximum bandwidth due to the damping factor γ^* is greatly reduced to 24.7 GHz, which is a direct result of the overdamping caused by the mode nonuniformity. Furthermore, the low-frequency roll-off due to f_p and f_q sets the actual maximum bandwidth even smaller, as observed in Fig. 4. Since our simulations with Minilase and the rate equation model have not included the nonlinear gain effects due to hot carriers and self-heating, the bandwidth of a real device may actually be further limited by the overall gain suppression effects. Nevertheless, the nonlinear effect due to mode

[3]As demonstrated from Minilase simulations in [12], some low-frequency roll-off can also be induced by the diffusion capacitance associated with the minority carriers.

[4]Note that g' is set to 1×10^{-19} m^2 for the InGaAs–AlGaAs QW in our simulations, which is large compared to 3.5×10^{-18} m^2 for the 1.3-μm InGaAsP system in [22].

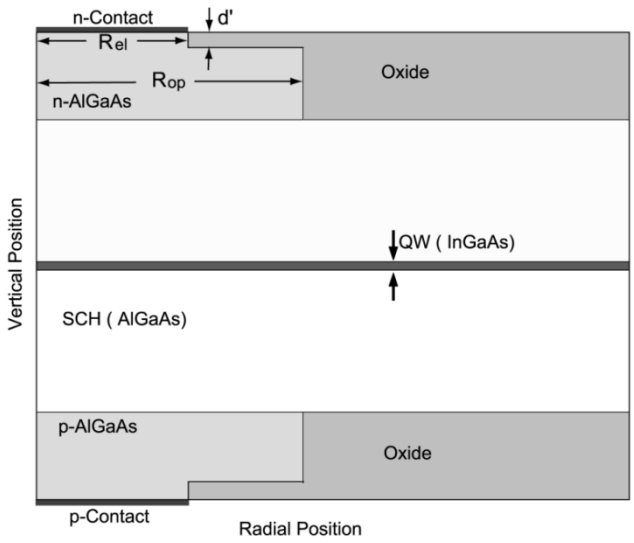

Fig. 7. Schematic plot of a VCSEL device with a tapered oxide aperture.

nonuniformity leads to an increase in the K factor and sets a limit on the maximum bandwidth that is comparable to those restricted by other gain suppression effects. Hence, this effect becomes a key factor for defining the high-speed performance of small aperture VCSELs. Another important issue is the role of the photon lifetime for this overdamping effect. Our simulations further demonstrate that the maximum bandwidth is increased by reducing the photon lifetime. Therefore, the limit on $f_{\max}$ due to mode nonuniformity might become less important for devices with very small photon lifetime. Since a smaller photon lifetime results in a larger threshold current, a tradeoff between low-threshold and maximum high-speed capacity is needed for device optimization.

It is possible to reduce the overdamping effect due to mode nonuniformity with careful device design and therefore improve the modulation bandwidth. The basic idea is to make the electrical aperture size smaller than that of the optical aperture, so that the current injection is more tightly confined to the peak region of the optical mode. In practice, such a design can be implemented by using a tapered oxide structure, which has been previously proposed to improve the steady-state performance of VCSELs [23]. We have been able to simulate the dynamic behavior of such complicated structures with Minilase. The schematic plot for a tapered aperture structure is shown in Fig. 7. It can be seen that a very thin layer of oxide placed at the optical field null extends toward the center and confines the current injection. Since the thin layer is placed at the field null, its influence on the optical field is very small. Therefore, we have used the same transverse optical mode and photon lifetime as for the case without thin oxide. For this tapered aperture device, the electrical aperture radius $R_{\rm el}$ is 1.2 μm and the optical aperture radius $R_{\rm op}$ is 1.8 μm. The thickness of the thin oxide layer (d',) is set to 20 nm, which is about 1/4 that of the quarter-wavelength oxide layer. A normal device with an abrupt oxide aperture is also simulated, for which $R_{\rm el} = R_{\rm op} = 1.8$ μm. Fig. 8(a) shows the simulated transverse-mode profile and the distribution of the current incident onto the QW from the p-side for both devices. All quantities are normalized with respect to their peak values.

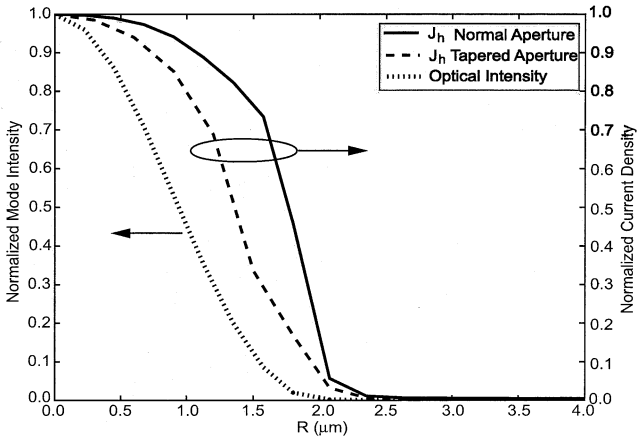

(a)

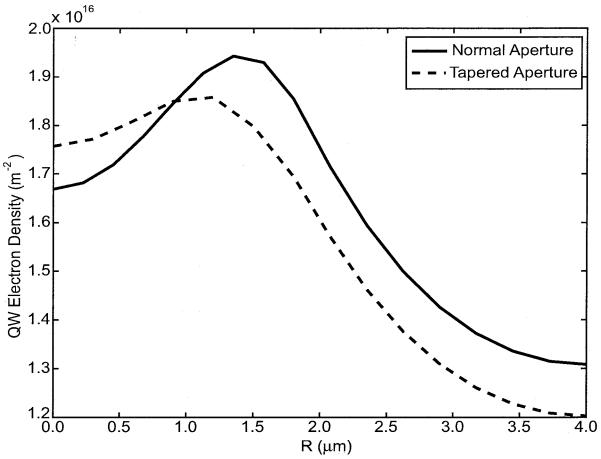

(b)

Fig. 8. Minilase simulation results. (a) Normalized transverse-mode profile and current density incident onto the QW from the p side. (b) Bound electron density distribution within the QW. Two devices are simulated at 0.10-mW output power: one with normal oxide aperture and $R_{\rm el} = R_{\rm op} = 1.8$ μm; the other with tapered oxide aperture for which $R_{\rm el} = 1.2$ μm and $R_{\rm op} = 1.8$ μm.

Both devices have the same transverse mode since their optical aperture has equal size. It is observed that a larger fraction of current is injected into the region where the optical intensity is small in the normal device. This is because the current injection varies slowly within the oxide aperture, while the optical mode intensity decays rapidly from center to the edge of the aperture due to the strong index guiding of the oxide. On the other hand, the overlap between the current injection and the optical mode is greatly enhanced for the tapered oxide device due to the fact that $R_{\rm el} < R_{\rm op}$. Fig. 8(b) shows the two-dimensional density profile of the bound electrons within the QW for the two devices. It is evident that SHB is less severe in the tapered aperture device, which is a direct result of the enhanced overlap between the current injection and the mode profile. The simulated response curves for both structures at the same output powers are plotted in Fig. 9. Although the difference in response curves is small at low bias, significant improvements in the modulation response are observed for the tapered oxide device at higher output power.

The above simulations demonstrate that high-speed performance requires minimal current injection into the tail region of the optical mode profile, because the carriers in that region respond slower to the modulation, as shown in Fig. 2. Conse-

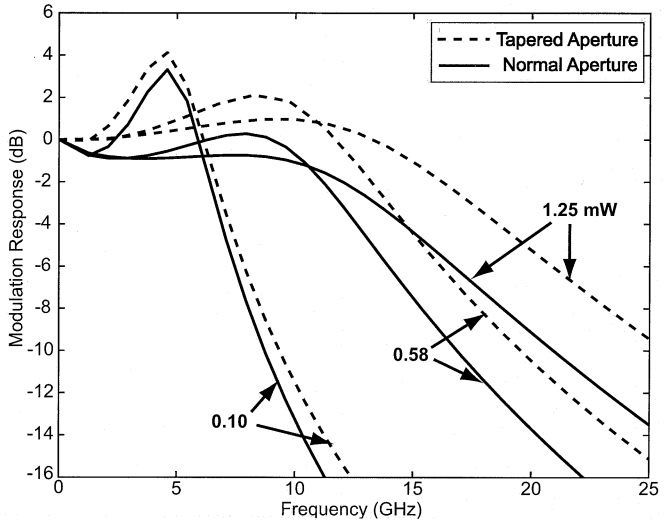

Fig. 9. Modulation responses simulated with Minilase for the two devices identical to those in Fig. 8. The response curves are marked by the output power.

quently, the modulation response will be very sensitive to the lateral diffusion of carriers in the SCH region, which is characterized by l_D in (4). The rate equation approach is, therefore, only useful for qualitative analysis, due to its inability to account for distributed carrier transport. Moreover, considering that the actual modulation response in a real device is determined by the overall combined effects of the nonuniform mode, the diffusion capacitance, hot-electron and self-heating, comprehensive VCSEL simulators such as Minilase become an absolute necessity for quantitative VCSEL device optimizations.

IV. Conclusion

Detailed studies have been carried out to investigate the effect of the nonuniformity of optical modes on the modulation response of VCSELs. Various oxide-confined VCSEL structures have been simulated with both the self-consistent laser diode simulator, Minilase, and a 1-D rate equation model. It has been clearly demonstrated that the transverse-mode nonuniformity leads to an overdamping and a low-frequency roll-off of the response curves of VCSELs, particularly those with small oxide apertures. These nonlinear effects are explained by the different dynamic behavior of QW carriers at different spatial locations. Due to the limit of this nonlinear effect, VCSELs exhibit a much lower maximum bandwidth than predicted by the conventional rate equation model. Furthermore, a possible device design with the electrical aperture smaller than the optical aperture has been discussed. It has been demonstrated that the nonlinear effect due to mode nonuniformity is greatly reduced by using a tapered oxide aperture, and hence this design improves the modulation bandwidth significantly.

Appendix
Analytical Solution for the Simplified 1-D Rate Equation Model

It is generally difficult to analytically solve the original 1-D rate equation model described in Section II, particularly due to the lateral diffusion term in the continuity equation. However, the lateral diffusion does not significantly affect the modulation bandwidth for reasonable carrier mobilities as discussed in Section III, and we will ignore this term in the following derivations. Another simplification we make is to assume a uniform current injection throughout the entire QW plane. This assumption is also a reasonably simplification for a realistic device with normal oxide aperture as shown in Fig. 8. We can then write the steady-state equations as

$$0 = \frac{J_0}{qd} - \frac{N_0}{\tau_r} - \alpha \cdot \eta \cdot v \cdot g' \cdot S_0(N_0 - n_{tr}) \tag{A.1}$$

and

$$0 = \Gamma_z \int_0^{R_D^2} \alpha \cdot v \cdot g' \cdot S_0(N_0 - n_{tr}) dr^2 / R_D^2 - \frac{S_0}{\tau_p}. \tag{A.2}$$

By solving these two linear equations, the expression for the steady-state carrier density as a function of position r is given by

$$N_0' \equiv N_0 - n_{tr} = \frac{R_D^2}{\Gamma_z \tau_p v_g g'} (1/\tau_r + \alpha\eta v_g g' S_0)^{-1} \cdot \left(\int_0^{R_D^2} \frac{\alpha}{1/\tau_r + \alpha\eta v_g g' S_0} dr^2 \right)^{-1}. \tag{A.3}$$

It is obvious from this expression that a larger spatial hole will be burned at the center as S_0 rises.

To obtain the expression for the modulation response, we perform a small signal analysis and assume $j(t) = J_0 + j(f) \cdot e^{i2\pi ft}$, $n(t) = N_0 + n(f) \cdot e^{i2\pi ft}$ and $s(t) = S_0 + s(f) \cdot e^{i2\pi ft}$. By substituting these relations into the rate equations [(2) and (3)] and equating the coefficients of $e^{i2\pi ft}$, the rate equations for the small signals are derived as

$$i2\pi f \cdot n(f) = \frac{j(f)}{qd} - \frac{n(f)}{\tau_r} - \alpha\eta v_g g' S_0 n(f) - \alpha\eta v_g g' s(f) N_0' \tag{A.4}$$

and

$$i2\pi f \cdot s(f) = \frac{\Gamma_z}{R_D^2} \int_0^{R_D^2} \alpha v_g g' S_0 n(f) \cdot dr^2. \tag{A.5}$$

The modulation response $R(f)$ is defined as the ratio of $s(f)/j(f)$ and can be extracted from the two equations above as in (A.6), shown at the bottom of the page.

As can be seen from (A.3) and (A.6), the solution for the modulation response can be obtained if the normalized

$$R(f) \equiv \frac{s(f)}{j(f)} = \frac{\Gamma_z v g' S_0}{R_D^2 qd} \int_0^{R_D^2} \frac{\alpha}{i2\pi f + \tau_r^{-1} + \alpha\eta v_g g' S_0} dr^2 \cdot \left[i2\pi f + \frac{\Gamma_z S_0 v_g^2 g'^2}{R_D^2} \cdot \int_0^{R_D^2} \frac{\alpha^2 N_0'}{i2\pi f + \tau_r^{-1} + \alpha\eta v_g g' S_0} dr^2 \right]^{-1}. \tag{A.6}$$

mode intensity α is specified. As described in Section II, it is a very good approximation to assume that the mode intensity is Gaussian-like, $\alpha = \theta \cdot \exp(-(r/R_w)^2)$, and $\theta = R_D^2/R_w^2 \cdot (1 - e^{-R_D^2/R_w^2})^{-1}$, which is determined by the normalization condition $\int_0^{R_D^2} \alpha \, dr^2/R_D^2 = 1$. Typically we have $R_D \gg R_w$, and therefore $\theta \approx R_D^2/R_w^2$ is obtained. For this Gaussian mode profile, we finally derive the analytical expression for the modulation response

$$\frac{s(f)}{j(f)} = \frac{\Gamma_z R_w^2}{qdR_D^2}\left[i2\pi f \cdot \ln\left(1+\frac{\theta\eta v_g g' S_0 \tau_r}{1+i2\pi f\tau_r}\right)^{-1} + \frac{i2\pi f+\tau_r^{-1}}{i2\pi f\tau_p} \cdot \ln(1+\theta\eta v_g g' S_0\tau_r)^{-1} - \frac{\tau_r^{-1}}{i2\pi f\tau_p} \cdot \ln\left(1+\frac{\theta\eta v_g g' S_0\tau_r}{1+i2\pi f\tau_r}\right)^{-1}\right]^{-1}. \quad \text{(A.7)}$$

For low output power (small S_0) one can perform a Taylor expansion of (A.7). To the first order, we have $\ln(1+x)^{-1} \approx 1/x + 1/2$ for $x \ll 1$. Hence, the modulation response for very low output power becomes

$$\frac{s(f)}{j(f)} \approx \frac{\Gamma_z v_g g' S_0}{qd}\left[\left(-4\pi^2 f^2 + \frac{1}{2}\,\frac{\theta\eta v_g g' S_0}{\tau_p}\right) + i2\pi f\left(\tau_r^{-1} + \tfrac{1}{2}\,\theta\eta v_g g' S_0\right)\right]^{-1} \quad \text{(A.8)}$$

which reduces to the result of the conventional rate equations shown in (1), except that S_0 is replaced by $\theta\eta S_0$ here. As the output power increases, higher order effects need to be considered. For the second order approximation, $\ln(1+x)^{-1} \approx 1/x + 1/2 - x/12$ for $x \ll 1$ and we can therefore write (A.7) in the form

$$\frac{s(f)}{j(f)} \propto \frac{P^{(1)}(i2\pi f)}{Q^{(3)}(i2\pi f)} \quad \text{(A.9)}$$

where $P^{(1)}(i2\pi f)$ and $Q^{(3)}(i2\pi f)$ are first- and third-order polynomials of $i2\pi f$ with real coefficients. In other words, the modulation response at high output power is a transfer function with one zero and three poles and can be expressed as

$$\frac{s(f)}{j(f)} \propto \frac{f - f_p}{f - f_q} \cdot \left[\left(f^2 - f_r^{*2}\right) - if\gamma^* \Big/ (2\pi)\right]^{-1} \quad \text{(A.10)}$$

where f_p, f_q, f_r^*, and γ^* are real quantities and can be obtained by fitting to the numerical simulation results.

ACKNOWLEDGMENT

The authors would like to thank Prof. S. L. Chuang and Prof. K. Choquette of the University of Illinois at Urbana-Champaign for very valuable discussions. The suggestion by the anonymous reviewer to calculate the effective nonlinear gain factor is also appreciated.

REFERENCES

[1] K. L. Lear, A. Mar, K. D. Choquette, S. P. Kilcoyne, R. P. Schneider, and K. M. Geib, "High-frequency modulation of oxide-confined vertical cavity surface emitting lasers," *Electron. Lett.*, vol. 32, pp. 457–458, 1996.

[2] J. W. Scott, B. J. Thibeault, C. J. Mahon, and L. A. Coldren, "High modulation efficiency of intracavity contacted vertical cavity lasers," *Appl. Phys. Lett.*, vol. 65, pp. 1483–1485, 1994.

[3] G. P. Agrawal, "Gain nonlinearities in semiconductor lasers: Theory and application to distributed feedback lasers," *IEEE J. Quantum Electron.*, vol. 6, pp. 860–868, 1987.

[4] W. Rideout, W. F. Sharfin, E. S. Koteles, M. O. Vassell, and B. Elman, "Well-barrier hole burnings in quantum well lasers," *IEEE Photon. Technol. Lett.*, vol. 3, pp. 784–786, 1991.

[5] R. Nagarajan, M. Ishikawa, T. Fukushima, R. S. Geels, and J. E. Bowers, "High speed quantum-well lasers and carrier transport effects," *IEEE J. Quantum Electron.*, vol. 28, pp. 1990–2007, 1992.

[6] M. Grupen and K. Hess, "Simulation of carrier transport and nonlinearities in quantum well laser diodes," *IEEE J. Quantum Electron.*, vol. 34, pp. 120–140, 1998.

[7] A. Valle, J. Sarma, and K. A. Shore, "Spatial holeburning effects on the dynamics of vertical cavity surface-emitting laser diodes," *IEEE J. Quantum Electron.*, vol. 31, pp. 1423–1431, 1995.

[8] Y. Satuby and M. Orenstein, "Mode-coupling effects on the small-signal modulation of multitransverse-mode vertical-cavity semiconductor lasers," *IEEE J. Quantum Electron.*, vol. 35, pp. 944–954, 1999.

[9] S. F. Yu, "Dynamic behavior of vertical-cavity surface-emitting lasers," *IEEE J. Quantum Electron.*, vol. 32, pp. 1168–1179, 1996.

[10] S. F. Yu, W. N. Wong, P. Shum, and E. H. Li, "Theoretical analysis of modulation response and second-order harmonic distortion in vertical-cavity surface-emitting lasers," *IEEE J. Quantum Electron.*, vol. 32, pp. 2139–2147, 1996.

[11] J. Feng, T. R. Chen, and A. Yariv, "Effects of nonuniform photon distribution on high speed response in semiconductor distributed feedback lasers," *Appl. Phys. Lett.*, vol. 67, pp. 3706–3708, 1995.

[12] Y. Liu, W.-C. Ng, F. Oyafuso, B. Klein, and K. Hess, "Simulating the modulation response of VCSELs: The effects of diffusion capacitance and spatial hole-burning," *Proc. Inst. Elect. Eng.—Optoelectronics*, vol. 149, pp. 182–188, 2002.

[13] Y. Liu, W.-C. Ng, F. Oyafuso, B. Klein, and K. Hess, "Simulating the effect of spatial hole burning on the modulation response of VCSELs," in *Proc. SPIE, Physics and Simulation of Optoelectronic Devices X*, vol. 4646, P. Blood, M. Osinski, and Y. Arakawa, Eds., 2002, pp. 190–198.

[14] F. A. Oyafuso, B. D. Klein, L. F. Register, and K. Hess, "Fully coupled electrical and optical simulation of VCSELs," in *Proc. SPIE, Vertical-Cavity Surface-Emitting Lasers IV*, vol. 3946, K. D. Choquette and C. Lei, Eds., 2000, pp. 108–116.

[15] S. L. Chuang, *Physics of Optoelectronic Devices*. New York: Wiley, 1995.

[16] L. A. Coldren and S. W. Corzine, *Diode Lasers and Photonic Integrated Circuits*. New York: Wiley, 1995.

[17] F. Oyafuso, P. von Allmen, M. Grupen, and K. Hess, "Inclusion of band-structure and many-body effects in a quantum well laser simulator," *VLSI Design*, vol. 8, pp. 463–468, 1998.

[18] B. Klein, L. F. Register, K. Hess, D. G. Deppe, and Q. Deng, "Self-consistent Green's function approach to the analysis of dielectrically apertured vertical-cavity surface-emitting lasers," *Appl. Phys. Lett.*, vol. 73, pp. 3324–3326, 1998.

[19] W.-C. Ng, Y. Liu, B. Klein, and K. Hess, "Improved effective index method for oxide-confined VCSEL mode analysis," in *Proc. SPIE, Physics and Simulation of Optoelectronic Devices X*, vol. 4646, P. Blood, M. Osinski, and Y. Arakawa, Eds., San Jose, CA, 2002, pp. 168–175.

[20] N. K. Dutta, "Analysis of current spreading, carrier diffusion, and transverse mode guiding in surface emitting lasers," *J. Appl. Phys.*, vol. 68, pp. 1961–1963, 1990.

[21] S. W. Corzine, R. S. Geels, J. W. Scott, R. H. Yan, and L. A. Coldren, "Design of Fabry–Perot surface-emitting lasers with a periodic gain structure," *IEEE J. Quantum Electron.*, vol. 25, pp. 1513–1524, 1989.

[22] R. Olshansky, P. Hill, V. Lanzisera, and W. Powazinik, "Universal relationship between resonant frequency and damping rate of 1.3 μm InGaAsP semiconductor lasers," *Appl. Phys. Lett.*, vol. 50, pp. 653–655, 1987.

[23] E. R. Hegblom, N. M. Margalit, A. Fiore, and L. A. Coldren, "High-performance small vertical-cavity lasers: A comparison of measured improvements in optical and current confinement in devices using tapered apertures," *IEEE J. Select. Topic Quantum Electron.*, vol. 5, pp. 553–560, 1999.

Yang Liu received the B.S. degree in physics from the University of Science and Technology of China, Hefei, China, in 1998. He is currently working toward the Ph.D. degree in physics at the University of Illinois at Urbana-Champaign.

His major research interests include semiconductor device physics and the modeling and simulation of optoelectronics.

Wei-Choon Ng (M'03) received the B.Eng. degree (with first-class honors) and the M.Eng. degree, both in electrical engineering, from the National University of Singapore (NUS) in 1996 and 1998 respectively. He is currently working toward the Ph.D. degree in electrical engineering with the Computational Electronics Group at the University of Illinois at Urbana–Champaign.

During 1995, he was with British Telecoms Labs, Ipswich, U.K., working on optical thin-film coating for industrial placement. His research interests mainly focus on semiconductor transport, thermal modeling of semiconductor lasers, modeling guided-wave devices and computation electromagnetics.

Mr. Ng is a Senior Research Fellow of the International Society for Philosophical Enquiry (ISPE) and a member of the Lasers and Electro-Optic Society (LEOS), the Antennas and Propagation Society (APS), and Phi Kappa Phi.

Benjamin Klein received the Ph.D. degree in electrical engineering from the University of Illinois at Urbana-Champaign in 2000.

He is currently with the National Institute of Standards and Technology, Boulder, CO.

Karl Hess (F'85) received the Ph.D. degree in applied physics from the University of Vienna, Vienna, Austria, in 1970.

Currently, he holds the Swanlund Endowed Chair and is a Professor of Electrical and Computer Engineering and Professor of Physics at the University of Illinois at Urbana-Champaign. He is also with the Beckman Institute, where his current research is in the area of molecular and electronic nanostructures. He has dedicated the major portion of his research to electronic transport in semiconductors and semiconductor devices, with particular emphasis on hot electron effects and effects pertinent to device miniaturization. He is particularly interested in problems that require large computational resources for their solution.

Dr. Hess has received numerous awards, including the IEEE J.J. Ebers Award of the Electron Devices Society in 1993 and the IEEE Sarnoff Field Award for Electronics in 1995. He is a Fellow of the American Physics Society, the American Association for the Advancement of Science, and the American Academy of Arts and Sciences, and a member of the National Academy of Engineering.